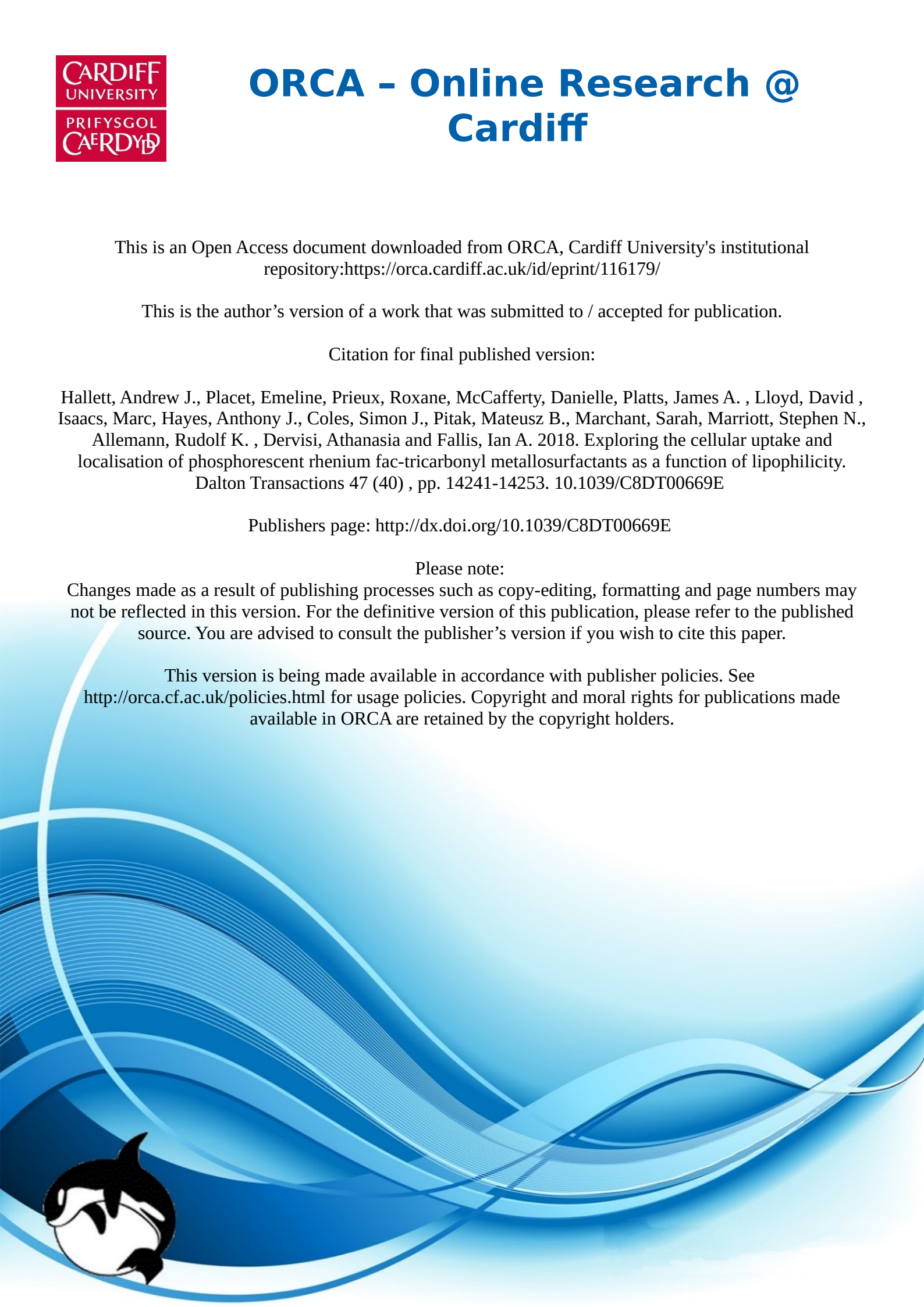

Exploring the cellular uptake and localisation of phosphorescent rhenium fac-tricarbonyl metallosurfactants as a function of lipophilicity†

Andrew J. Hallett,*[a] Emeline Placet,[a] Roxane Prieux,[a] Danielle McCaffery,[a] James A. Platts,[a] David Lloyd,[b] Marc Isaacs,[c] Anthony J. Hayes,[c] Simon J. Coles,[d] Mateusz B. Pitak,[d] Sarah Marchant,[e] Stephen N. Marriott,[e] Rudolf K. Allemann,[a] Athanasia Dervisi*[a] and Ian A. Fallis*[a]

A systematic study of the cellular uptake of emissive complexes as a function of their lipophilicity is presented. Here a series of amphiphilic rhenium fac-tricarbonyl bisimine complexes bearing axial substituted imidazole or thiazole ligands, $[Re(bpy)(CO)_3(ImC_nH_m)]^+$ {n = 1 m = 3 (1^+), n = 4 m = 9 (2^+), n = 8 m = 17 (3^+), n = 12 m = 25 (4^+), n = 16 m = 33 (5^+), n = 2 m = 3 (6^+); bpy = 2,2'-bipyridine, Im = imidazole} and $[Re(bpy)(CO)_3(L)]^+$ {L = 1-mesitylimidazole, ImMes (7^+), 4,5-dimethylthiazole, dmt (8^+) and 4-methyl-5-thiazole-ethanol, mte (9^+)} is reported. The X-ray crystal structures of 2^+, 8^+ and 9^+ confirm the geometry and expected distribution of ligands and indicated that the plane of the imidazole/thiazole ring is approximately parallel to the long axis of the bipy ligand. Luminescence studies revealed excellent properties for their use in cell imaging with visible excitation and broad emission profiles. Their uptake in two distinct species has been examined by fluorescence imaging of the diplomonad fish parasite Spironucleus vortens (S. vortens) and rod-shaped yeast Schizosaccharomyces pombe (Schiz. pombe) as a function of their lipophilicity. The uptake of the complexes was highest for the more lipophilic 2^+–5^+ in both S. vortens and Schiz. pombe in which the long alkyl chain aids in crossing bilipid membranes. However, the increased lipophilicity of longer chains also resulted in greater toxicity. Localisation over the whole cell varied with differing alkyl chain lengths with complex 2^+ preferentially locating to the nucleus of S. vortens, 3^+ showing enhanced nuclear partitioning in Schiz. pombe, and 4^+ for the remaining cell wall bound in the case of S. vortens. Interestingly, complexes of intermediate lipophilicity such as 7^+ and 8^+ showed reason-able uptake, proved to be non-toxic, and were capable of crossing exterior cell walls and localising in the organelles of the cells.

Introduction

Surface active metal complexes, known as metallosurfactants,[1] may be defined as amphiphilic species in which the polar 'head-group' of a surfactant incorporates a metal complex. While 'standard' surfactants have found ubiquitous appli-cations in industrial, medical and domestic scenarios for many decades, metallosurfactants are a relatively new class of material. Since the lipophilicity of a metallosurfactant may be readily varied by changes in the size of the hydrophobic component of the amphiphilic structure,[2] we have chosen to examine the potential suitability of a range of phosphorescent rhenium(ı) fac-tricarbonyl metallosurfactants as cellular imaging agents. Phosphorescent complexes of the fac-$[Re^I(CO)_3(N\text{–}N)]$ {(N–N) = bis-imine ligand}[3] and in particular amphiphilic complexes[4] have been extensively studied for their luminescent properties, including recent applications, along

[a]School of Chemistry, Main Building, Cardiff University, Cardiff CF10 3AT, UK. E-mail: fallis@cardiff.ac.uk, hallettaj@cardiff.ac.uk, DervisiA@Cardiff.ac.uk; Fax: +44 (0)29-20874030; Tel: +44 (0)29-20879316

[b]Cardiff School of Biosciences, Main Building, Museum Avenue, Cardiff, CF10 3AT, UK

[c]Confocal Microscopy Unit, Cardiff School of Biosciences, Life Sciences Building, Cardiff, CF10 3US, UK

[d]UK National Crystallographic Service, Chemistry, Faculty of Natural and Environmental Sciences, University of Southampton, Highfield, Southampton, SO17 1BJ, UK

[e]Defence Science Technology Laboratory, (DSTL), Porton Down, Salisbury, SP4 0JQ, UK

†Electronic supplementary information (ESI) available: cif file, full tables of crystallographic data, luminescence spectra for all compounds and images of con-focal microscopy. CCDC 969748, 990428 and 990429. For ESI and crystallo-graphic data in CIF or other electronic format see DOI: 10.1039/c8dt00669e

with Ru^{II} and Ir^{III} complexes, as phosphors in live-cell imaging confocal fluorescence microscopy.[5] Variation of the bis-imine or the axial ligands greatly influences the properties of the complexes such as solubility, stability, cytotoxicity, lifetimes, cellular uptake, membrane permeability and organelle localis-ation within the cells. Their ease of visible excitation, large Stokes shifts and long-lived ^{3}MLCT excited states, promoted by heavy metal assisted spin–orbit coupling and inter-system crossing, aid in distinguishing between emission from the complexes and that of matrix auto-fluorescence, thus improv-ing contrast in confocal imaging work. In addition, selective imaging can be achieved by noting that the photophysical pro-perties of this type of material are microenvironment sensi-tive.[6] Tricarbonyl complexes have also proven useful in imaging within parasites.[7] Whilst many metal-based cellular imaging probes are now employed to great effect, their localis-ation within cells is a complex function of both their physical properties and reactivity, and thus their effective design can be somewhat serendipitous. As an aid to the rational design of these materials we felt it to be valuable to systematically vary the lipophilicity of a model system to determine the effect of hydrophobicity on the biodistribution of metal based phos-phors. In addition, Re complexes are attracting much attention as potential chemotherapeutic agents,[8] while the beta emitters ^{186}Re and ^{188}Re are potentially useful radiotherapeutic iso-topes.[9] Hence understanding how to modulate rhenium cellu-lar distribution is of particular medicinal value.

Long chain methylimidazolium compounds are amphi-philic, which is they possess an organic hydrophobic chain termi-nated with a polar head group. These compounds have been extensively studied as surfactants,[10] ionic liquids,[11] liquid crys-tals[12] and as precursors to N-heterocyclic carbenes.[13] In the current paper the methyl group has been replaced by the cat-ionic fac-{$Re^I(CO)_3(N–N)$} moiety to afford a range of phosphor-escent complexes, bearing varying alkyl, vinyl and aromatic groups. The longer alkyl chain variants are metallosurfactants and are suited to penetrate into the lipid bilayer of live cells with the cationic nature assisting crossing membranes via passive diffusion. Here, the uptake and localisation of the complexes was examined as a function of the complex lipo-philicity by confocal fluorescence imaging using two micro-organisms, namely the diplomonad fish parasite Spironucleus vortens (S. vortens) and rod-shaped yeast Schizosaccharomyces pombe (Schiz. pombe).

Results and discussion

Synthesis and characterisation of the ligands and complexes

The 1-alkylimidazole ligands (ImC_4H_9, ImC_8H_{17}, $ImC_{12}H_{25}$ and $ImC_{16}H_{33}$) were prepared in good yields (~85%) by react-ing imidazole with 1 molar equivalent of the appropriate bromoalkane in DMF at 120 °C in the presence of base. After aqueous work-up, the ligands were purified by bulb-to-bulb vacuum distillation using a Kügelrohr apparatus. The mesityl substituted ligand, ImMes, was synthesised by reacting 2,4,6-trimethylaniline, glyoxal and formaldehyde in the presence of NH_4Cl according to a literature procedure.[14] Again the product was purified by bulb-to-bulb vacuum distillation using a Kügelrohr apparatus. All other ligands are commercially available.

Reaction of the imidazole/thiazole ligands with the precur-sor complex $[Re(CO)_3(bpy)(NCMe)]BF_4$ in hot $CHCl_3$ for 16 h, followed by purification by column chromatography led to the complexes $[Re(CO)_3(bpy)L]BF_4$ (Fig. 1) 1^+–9^+ in moderate to good yields (61–93%) as bright yellow powders. The complexes were characterised by ^{1}H and ^{13}C–{^{1}H} NMR spectroscopy, low and high resolution electrospray mass spectrometry, HPLC, IR, UV-vis and fluorescence spectroscopies and elemental analysis. The complexes 1^+ and 7^+ have been previously reported as the PF_6^- and OTf^- salts for study of the energy gap law[15,29] and C–N bond cleavage of the bipyridine[16] respect-ively; however, characterisation data are included in the Experimental section for comparison and completeness.

For reasons of synthetic accessibility, we adopted this 3 car-bonyl, chelating bis-imine plus an axial ligand approach. It should be noted however that such complexes may well undergo loss of the axial ligand as demonstrated by Leonidova et al.[17] and that these complexes are likely to be less stable than those of comparable tridentate ligands.[18] ^{1}H NMR spec-troscopy confirmed the coordination of the axial ligand in each case with, for example, an upfield shift of the sharp imid-azole moiety resonances of ImC_4H_9 from 7.41, 6.99 and 6.84 ppm in the free ligand to broad singlets at 6.93, 6.78 and 6.73 ppm in 2^+. In addition, the sharp imidazole resonances of ImMes show an upfield shift from 7.47, 7.27 and 6.93 ppm in the free ligand to broad singlets at 7.20, 6.83 and 6.58 ppm in 7^+. It is noteworthy that the thiazole ligand mte, the axial ligand of complex 9^+, is a component of thiamine (vitamin B_1) when alkylated by a methylene bridged aminopyrimidine to form a cationic species (analogous to the cationic rhenium complexes here). Uptake of thiamine by cells of the blood and other tissues is believed to occur via active transport and passive diffusion.[19] This inexpensive thiazole has also found

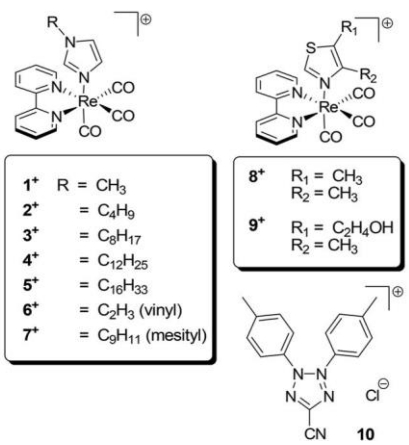

Fig. 1 The complexes $[Re(CO)_3(bpy)L]^+$ 1^+–9^+ in this study and the structure of ctc (10).

use as a food additive. Here, its coordination to rhenium results in an upfield shift of the sharp thiazole moiety reso-nance in the ^{1}H NMR spectrum from 8.39 ppm in the free ligand to 7.88 ppm in complex 9^+, along with a downfield shift of the methyl resonance from 2.24 ppm in the free ligand to 2.37 ppm in 9^+, whilst leaving the resonances of the two methylene groups virtually unchanged. Solid-state IR studies (as KBr discs) of the complexes revealed two absorption bands between 2030 and 1910 cm^{-1} for the rhenium bound carbonyl stretches consistent with pseudo C_{3v} symmetry; a broader band at ca. 1920 cm^{-1} consists of two merged bands as seen in many previous examples.[3–5] Both low and high resolution mass spectrometry were obtained in which the correct isotopic distribution was observed for the monocationic species $[M - BF_4]^+$ in each case. The purity of the complexes was confirmed by elemental analysis with the expected composition with 4^+ being observed as a 1 : 3 Et_2O solvate.

X-ray crystallography studies

Yellow columnar crystals of $[Re(CO)_3(bpy)(ImC_4H_9)]BF_4$ 2^+, columnar crystals of $[Re(CO)_3(bpy)(dmt)]BF_4$ 8^+ (as a $CHCl_3$ solvate) and prismatic crystals of $[Re(CO)_3(bpy)(mte)]OTf$ 9^+ (grown as the triflate salt from an alternate sample) suitable for X-ray diffraction studies were grown by slow vapour diffusion of Et_2O into a concentrated solution of the complex in $CHCl_3$. The lattice parameters, data collection and structure refinement details are shown in Table 1 with selected bond lengths and angles reported in Table 2 (Fig. 2).

The crystallographic studies confirmed the proposed for-mulation with fac-coordination of the three carbonyl ligands, chelating bipyridine and the imidazole/thiazole ligand co-ordinated in the axial position {Fig. 3(a)–(c)}. In accordance with numerous related fac-rhenium tricarbonyl structures the complex shows distorted octahedral geometry around the metal centre with generally typical bond lengths for co-ordinated bipyridine and axial N-donor ligands.[3–5] The Re(1)– N(3) bond lengths {2.179(2), 2.243(2) and 2.231(6) Å for 2^+, 8^+ and 9^+ respectively}are longer than Re(1)–N(1) {2.169(2), 2.188
(3) and 2.188(5) Å}and Re(1)–N(2) {2.171(2), 2.177(3) and 2.174
(5) Å} bond lengths for all three complexes, particularly for thiazole complexes, 8^+ and 9^+ in which the difference is more pronounced. This is consistent with the reported structure of the imidazole based guanine complex $[Re(CO)_3(bpy)(gua)]^+$, the only structurally characterised example of a fac-rhenium
tricarbonyl complex with 2,2′-bipyridine and an axial imid-azole ligand.[20] However, the only other example of a fac-rhenium tricarbonyl complex bearing an axial imidazole
ligand (i.e. R = H from Fig. 1), which has 1,10-phenanthroline as the diimine ligand, $[Re(CO)_3(phen)(ImH)]^+$, does not show extended $Re–N_{axial}$ bond lengths and displays three essentially identical Re–N bond lengths.[21] The structures of 8^+ and 9^+ described here are the first reported structures of fac-rhenium tricarbonyl complexes bearing axial thiazole ligands. The
Re(1)–N(1) bond lengths in thiazole complexes {2.188(3) and 2.188(5) Å for 8^+ and 9^+ respectively} are longer than the imid-azole complex 2^+ {2.169(2) Å}. In addition, the Re(1)–N(3) bond lengths are considerably longer in the thiazole complexes

Table 1 Single crystal diffraction data parameters for $[Re(CO)_3(bpy)(ImC_4H_9)]BF_4$ (2^+), $[Re(CO)_3(bpy)(mte)]OTf$ (8^+) and $[Re(CO)_3(bpy)(mte)]OTf$ (9^+)

	$[Re(CO)_3(bpy)(ImC_4H_9)]BF_4$ 2^+	$[Re(CO)_3(bpy)(dmt)]BF_4$ 8^+	$[Re(CO)_3(bpy)(mte)]OTf$ 9^+ [a]
CCDC depository number	969748	990428	990429
Formula	$C_{20}H_{20}BF_4N_4O_3Re$	$C_{19}H_{16}BCl_3F_4N_3O_3ReS$	$C_{20}H_{17}F_3N_3O_7ReS_2$
Formula weight	637.41	745.77	718.69
Temperature/K	100(2)	100(2)	100(2)
Wavelength/Å	0.71075	0.71075	0.71075
Crystal size/mm^3	0.420 × 0.060 × 0.040	0.280 × 0.050 × 0.040	0.12 × 0.10 × 0.04
Crystal system	Monoclinic	Monoclinic	Orthorhombic
Space group	$P2_1/n$	$P2_1/c$	$P2_12_12_1$
a/Å	11.1861(6)	11.0109(8)	12.1102(9)
b/Å	12.2320(5)	17.8468(13)	13.1182(9)
c/Å	16.1257(11)	13.4164(9)	14.8639(10)
α/°	90.00	90.00	90.00
β/°	95.466(7)	111.137(2)	90.00
γ/°	90.00	90.00	90.00
Volume/$Å^3$	2196.4(2)	2459.1(3)	2361.3(3)
Z	4	4	4
F000	1232	1432	1392
μ/mm^{-1}	5.597	5.411	5.394
θ range for data collection	3.036 − 27.482°	3.024 − 27.476°	2.67 − 27.51°
Index ranges	−14 ≤ h ≤ 14, −15 ≤ k ≤ 11, −13 ≤ l ≤ 20	−14 ≤ h ≤ 14, −23 ≤ k ≤ 22, −17 ≤ l ≤ 15	−15 ≤ h ≤ 15, −17 ≤ k ≤ 11, −19 ≤ l ≤ 12
Reflections collected	15 288	17 474	18 399
Independent reflections (R_{int})	5016 (0.0287)	5579 (0.0471)	5408(0.0307)
Final R indices [$F^2 > 2\sigma(F^2)$]: R_1, wR_2	0.0201, 0.0494	0.0300, 0.0842	0.0258, 0.0658
R indices (all data)	0.0219, 0.0501	0.0317, 0.0854	0.0261, 0.0660

[a] Structure is a racemic twin ~40 : 60 ratio. Flack parameter = 0.371(3).[22]

Table 2 Selected bond lengths (Å) and angles (°) for $[Re(CO)_3(bpy)(ImC_4H_9)]BF_4$ (2^+), $[Re(CO)_3(bpy)(mte)]OTf$ (8^+) and $[Re(CO)_3(bpy)(mte)]OTf$ (9^+) and the values calculated from DFT studies for the model complexes 1^+ and 8^+

Bond length (Å)/angle (°)	2^+	Calculated values	8^+	9^+	Calculated values
Re(1)–N(1)	2.169(2)	2.185	2.188(3)	2.188(5)	2.189
Re(1)–N(2)	2.171(2)	2.185	2.177(3)	2.174(5)	2.188
Re(1)–N(3)	2.179(2)	2.213	2.243(2)	2.231(6)	2.255
Re(1)–C(11)	1.929(3)	1.925	1.933(3)	1.938(7)	1.923
Re(1)–C(12)	1.922(3)	1.925	1.937(4)	1.930(8)	1.923
Re(1)–C(13)	1.926(3)	1.931	1.924(3)	1.926(7)	1.927
C(11)–O(1)	1.145(3)	1.157	1.142(4)	1.144(9)	1.158
C(12)–O(2)	1.145(3)	1.157	1.140(5)	1.146(9)	1.158
C(13)–O(3)	1.149(3)	1.155	1.148(4)	1.138(8)	1.154
N(3)–C(14)	1.329(3)	1.334	1.314(4)	1.324(9)	1.323
N(4)/S(1)–C(14)	1.341(3)	1.355	1.695(3)	1.681(7)	1.707
N(1)–Re(1)–C(11)	174.78(9)	172.07	172.8(1)	174.9(3)	171.75
N(2)–Re(1)–C(12)	171.94(9)	172.07	175.4(1)	174.0(3)	171.72
N(3)–Re(1)–C(13)	176.60(9)	178.99	177.0(1)	175.5(3)	177.13
C(11)–Re(1)–C(12)	86.85(11)	90.12	86.35(1)	85.3(3)	91.02

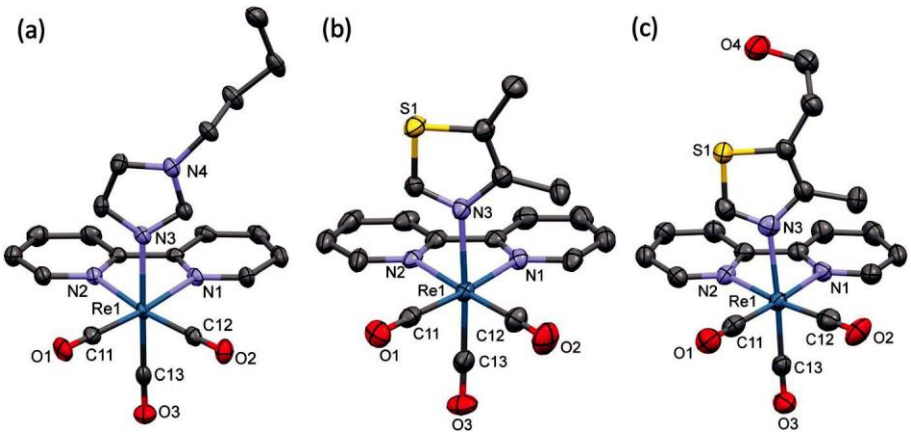

Fig. 2 Cation structure and atom labelling scheme of (a) $[Re(CO)_3(bpy)(ImC_4H_9)]$ (2^+) and (b) $[Re(CO)_3(bpy)(dmt)]$ (8^+) and (c) $[Re(CO)_3(bpy)(mte)]$ (9^+) (displacement ellipsoids are at 70% probability, hydrogen atoms and counter ions are removed for clarity).

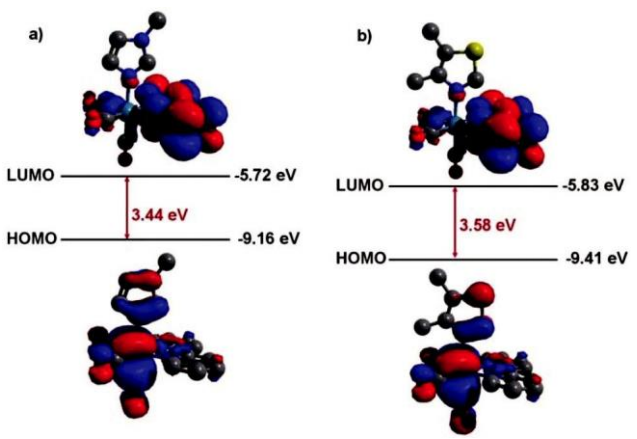

Fig. 3 Frontier orbitals of (a) $[Re(CO)_3(bpy)(ImCH_3)]^+$ 1^+ and (b) $[Re(CO)_3(bpy)(dmt)]^+$ 8^+.

{2.243(2) and 2.231(6) Å respectively} than the imidazole complex {2.179(2) Å}. However, the Re(1)–N(2) bond lengths are indistinguishable. The Re–C_{axial} and Re–$C_{equatorial}$ bond lengths are essentially identical in all three complexes, as are the C–O bonds.

In each case, the heterocyclic (imidazole or thiazole) axial donor ligands are positioned mutually perpendicular to the plane of the bipyridine ligand (i.e. mutually parallel to the 2,2′,5,5′-position of the bipyridine). The N(4)–C(14) bond of 2^+ {1.341(3) Å} is shorter than the S(1)–C(14) bonds of 8^+ {1.695(3) Å} and 9^+ {1.681(7) Å} reflecting the delocalised aromatic nature of the imidazole ligands compared with the thiazole ligands. Interestingly, for 9^+ the bipyridine ligand is slightly tilted with the N(3)–Re(1)–N(2) angle {88.49(15)°} much larger than the N(3)–Re(1)–N(1) angle {81.63(15)°}.

The bond lengths and angles of 2^+, 8^+ and 9^+ were com-pared with the optimised values calculated from density func-tional theory (DFT) for structurally simplified models (Table 2). In general, a reasonable agreement is obtained between the theoretical and experimentally observed bond lengths, although some small differences are found. The calcu-lated Re–$N_{bipyridine}$ bond lengths are longer for 2^+ (2.185 Å) with Re(1)–N(1) {2.169(2) Å} and Re(1)–N(2) {2.171(2) Å} 0.016 and 0.014 Å shorter. In addition, the calculated Re–N_{axial} bond

lengths are longer for 2^+ (2.213 Å) with Re(1)–N(3) {2.179(2) Å} 0.034 Å shorter. In the case of the thiazole complexes 8^+ and 9^+, there is excellent agreement of Re–N bond lengths between calculated values and experimental values. All Re–N bonds are predicted to be longer for the thiazole complexes than for the imidazole complex as seen experimentally.

The surface activity of the complexes could not be directly measured due to insufficient solubility in aqueous media, pre-cluding the determination of critical micelle concentrations. Further lipophilicity could not be measured via, for example, octanol/water partition coefficient measurements due to a weakly emulsifying nature of the metallosurfactant species. Thus to generate a quantitative measure of the complex hydro-philic or lipophilic character we calculated the surface area of the polar and non-polar components. Approximate structures of all nine cationic complexes were manually constructed from X-ray of 2^+ and 8^+, and geometry of the isolated cation fully optimised using the PM6-DH2 method[23] as implemented within MOPAC2012.[24] Coordinates were extracted, and used as input for a locally modified[25] version of MOLVOL[26] in order to calculate molecular volume and surface area data. This version automatically assigns van der Waals radii to all atoms, using standard values for C, H, O, N and S and a default value of 2 Å for Re. Table 3 reports values calculated in this manner. Here we see as expected the more surface active species have a higher total : polar area. The consequences of this are reflected below in the cellular uptake studies.

Electronic structure and spectroscopy

In order to determine the nature of the electronic transitions within this class of complex, DFT calculations (computed using the B3PW91 hybrid functional) were performed of the structurally simplified complexes of $ImCH_3$ 1^+ and dmt 8^+. In these examples, an assessment of the frontier orbitals pro-vided a qualitative insight into the HOMO (Highest Occupied Molecular Orbital) and LUMO (Lowest Unoccupied Molecular Orbital) energy levels. For the amide-functionalized complexes described here the energy levels of both the HOMO and LUMO are sufficiently different ($\Delta E > 0.2$ eV) from the other MOs to be considered independent. Population analyses revealed that the distribution of the frontier orbitals over the various ligands and metal is very similar in each case. The HOMOs (E = −9.16 and −9.41 eV respectively) are mainly situated on Re (ca. 60%), the three carbonyl ligands (ca. 24%) and imidazole/ thiazole (ca. 10%) whilst the LUMOs (E = −5.72 and −5.83 eV respectively) are located primarily on the bpy ligand (ca. 90%). The pictorial representations and relative distributions of the frontier orbitals are shown in Fig. 3 and Table 4, respectively.

The mixed metal/ligand character is consistent with pre-vious descriptions for complexes of this type[27] and suggests an excited state delocalised positive hole. The results suggest the lowest energy absorption should be reported as a HOMO → π* (bpy), in turn suggesting that significant MLCT and LLCT char-acter be predicted for the lowest energy excited state. The absorption spectra for the complexes show two main features with ligand-centred transitions dominating <320 nm and broad visible absorption at 330–450 nm associated with LLCT/ MLCT character (Fig. 4, Table 5).

The room temperature luminescence properties of com-plexes 1^+–9^+ were assessed in (aerated) $CHCl_3$ and DMSO/water (2 : 98), the solvent mixture used for confocal microscopy

Table 3 Volume (Å^3), total surface area, polar surface area and non-polar surface area (all Å^2)

Complex	Volume	Total surface area	Polar surface area	Non-polar surface area	Total : polar area
1^+	402.67	395.95	75.92	320.03	5.2
2^+	473.07	467.14	74.93	392.20	6.2
3^+	567.54	564.21	74.84	489.37	7.5
4^+	662.16	661.36	74.88	586.48	8.8
5^+	756.73	758.49	74.84	683.66	10.1
6^+	416.23	407.33	75.91	331.42	5.4
7^+	542.39	526.87	72.71	454.16	7.2
8^+	427.04	403.87	100.29	303.58	4.0
9^+	457.30	431.53	100.67	330.86	4.3

Table 4 Percentage distribution of HOMO and LUMO over complexes

	$[Re(CO)_3(bpy)(ImCH_3)]^+$ 1^+		$[Re(CO)_3(bpy)(dmt)]^+$ 8^+	
	HOMO	LUMO	HOMO	LUMO
Re	61.0	3.7	60.2	3.6
$ImCH_3$/dmt	9.6	2.8	9.5	3.2
CO (eq 1)	6.0	1.1	6.3	1.2
CO (eq 2)	6.0	1.1	6.5	1.1
CO (ax)	11.9	0.9	11.5	0.9
bpy	5.5	90.4	5.9	90.1

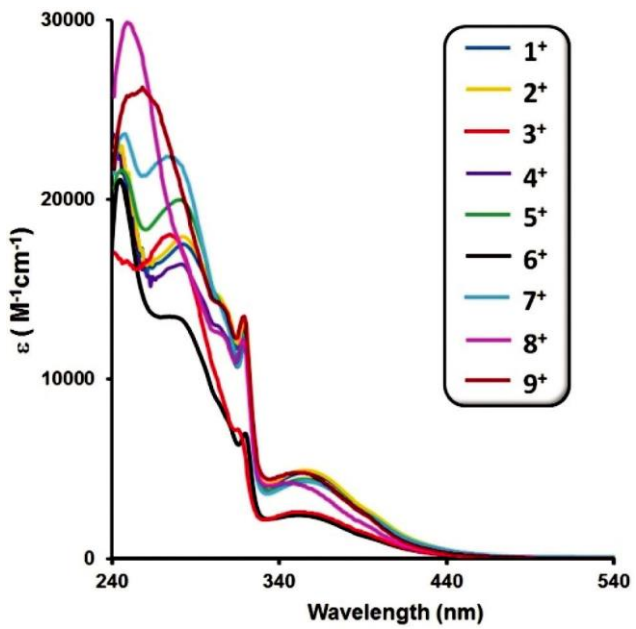

Fig. 4 UV-vis spectra of complexes 1^+–9^+ as $CHCl_3$ solutions (5×10^{-5} M).

Table 5 Photophysical properties of rhenium complexes 1^+–9^+

Compound	λ_{max} (ε/L mol^{-1} cm^{-1})[a]/nm	λ_{ex} $CHCl_3$ (H_2O)[b]/nm	λ_{em} $CHCl_3$/nm (τ aerated[c]/ns)	λ_{em} H_2O/nm[b] (τ aerated[c]/ns)
1^+	240 (22 900), 282 (17 525), 355 (4800)	404 (368)	568 (70)	580 (22)
2^+	240 (22 650), 282 (17 950), 355 (4915)	372 (366)	571 (65)	579 (28)
3^+	240 (17 400), 276 (18 050), 354 (2600)	383 (368)	571 (67)	568 (29)
4^+	240 (23 650), 282 (16 420), 354 (4350)	369 (365)	571 (63)	564 (42)
5^+	246 (21 650), 282 (20 000), 355 (4450)	366 (366)	573 (62)	534 (497)
6^+	245 (21 125), 276 (13 475), 351 (2400)	369 (360)	568 (83)	577 (33)
7^+	248 (23 675), 273 (22 425), 356 (4300)	362 (361)	561 (92)	558 (24)
8^+	251 (30 000), 346 (4225)	366 (360)	542 (308)	556 (96)
9^+	253 (25 975), 353 (4800)	365 (360)	552 (244)	556 (107)

[a] Measured as $CHCl_3$ solutions (5×10^{-5} M). [b] Measured as a DMSO/water (2 : 98) solution. [c] Excitation wavelength of 372 nm.

studies. The imidazole complexes 1^+–7^+ were emissive around 570 nm in $CHCl_3$. The relatively long lifetimes ($CHCl_3$, τ = 62–92 ns) are attributed to the MLCT/LLCT character, as dis-cussed in the context of the DFT results. The thiazole com-plexes 8^+ and 9^+ show substantially blue shifted emission (at ca. 540–550 nm), possibly due to the electron poor nature of the axial donors, as seen in the longer Re–N bond lengths in the thiazole versus imidazole structures (thiazoles generally react slowly with electrophiles, e.g. nitration, in comparison to imidazoles[28]). In addition the thiazole based complexes exhibit significantly extended lifetimes (308 and 244 ns respectively). It therefore appears that the thiazole axial ligands do not present the number of quenching pathways as the imidazole analogues. When the luminescence properties are studied in aerated aqueous conditions (water/DMSO 98 : 2) the characteristics are much more dependent on the amphi-philic nature of the compounds. For the complexes of the least lipophilic ligands 1^+, 2^+, 6^+, 8^+ and 9^+ the emission is red shifted by ca. 5–15 nm compared to that in $CHCl_3$. The lumi-nescent lifetimes are shorter lived, 20–30 ns for the imidazole complexes and 96–107 ns for the thiazole complexes. In more polar solvents, such as water (dielectric constants: water 80; $CHCl_3$ 5) stabilise dipolar CT excited states resulting in red-shifted emission.[29] For the slightly longer chain variants (and moderately lipophilic ligands) 3^+, 4^+ and 7^+ the emission is blue shifted by ca. 5 nm compared to that in $CHCl_3$, whilst the luminescent lifetimes remain shorter lived at 30–40 ns. Interestingly, for the imidazole complexes bearing the longest (hexadecyl) lipophilic chain 5^+, both the steady state and emis-sion lifetime properties show profound changes, the emission is blue shifted by 39 nm compared to that in $CHCl_3$ (Fig. 5) with an associated luminescent lifetime of 497 ns, suggesting that the ^{3}MLCT state is destabilised in water, raising the π* energy and thus the dπ–π* separation. It was previously noted that complexes bearing ligands incorporating long alkyl chains were able to 'wrap' the lipophilic chain around the complex, under aqueous conditions, protecting the bipyridine unit from the water. Both the blue shift in emission and the longer life-time suggest that the excited state is shielded from solvent quenching eff ects.[30] Overall, these characteristic absorption and emission properties, with the absorption maxima around 355 nm (tailing away to 440 nm), along with broad emission

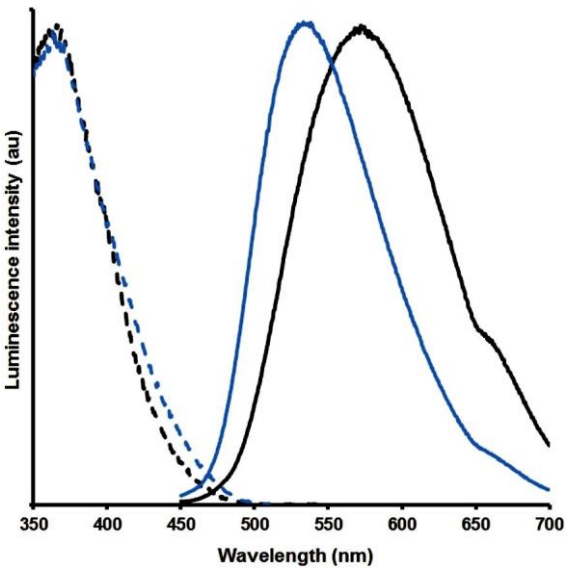

Fig. 5 Excitation (dashed) and emission (solid) spectra for [Re(CO)$_3$(bpy)(ImC$_{16}$H$_{33}$)]$^+$ 5^+ in $CHCl_3$ (black) and water/DMSO (98 : 2) (blue).

(450–730 nm) render these complexes highly compatible with confocal fluorescence microscopy.

Confocal fluorescence microscopy

Confocal fluorescence microscopy was used to study the fluo-rescence imaging capability of the complexes (1^+–9^+) using two diff ering cells, the anaerobically grown aerotolerant protistan fish parasite Spironucleus vortens (S. vortens) and unicellular eukaryote "fission yeast" Schizosaccharomyces pombe (Schiz. pombe). The diplomonad fish protist, S. vortens inhabits the gut as a parasite of ornamental fish (e.g. Angel fish), where O_2 partial pressures are low. During evolution they have lost the machinery of fully aerobic organisms (e.g. the rod-shaped yeast Schiz. pombe). Thereby mitochondria carrying out oxi-dative phosphorylation as a mechanism for energy production have evolved into a dihydrogen producing organelle, the hydro-genosome. Another major diff erence is that the protist, lacks the rigid, clearly defined multi-layered, rod-shaped cell wall

characteristic of the immotile yeast, and has instead a protein-phospholipid plasma membrane covered with highly flexible and structured glycoprotein-calyx. The parasite propels itself forward, driven by eight flagella. Whereas the yeast grows until it becomes a fourteen micrometer long cylinder then divides transversely to form a pair of short rods, the halving of cell volume by cell division and development of new flagella in the diplomonad is more complex. These contrasting and changing morphological characteristics during growth and development are revealed by the imaging techniques employing the more appropriate of the novel lumophores described here. In all cases an excitation wavelength of 405 nm was used together with a detection wavelength between 515–600 nm. Selected images of confocal fluorescence microscopy studies are pre-sented here, with all images available in the ESI.†

Firstly, the imidazole complexes which incorporate CH_3 1^+ and C_2H_3 (vinyl) 6^+ groups, the least lipophilic of the com-plexes, are not readily taken up intracellularly and are there-fore not toxic to S. vortens. Complex 1^+ was mounted in 'Vectashield' (an anti-fade mounting medium) containing the DNA/RNA-binding probe DAPI (4′,6-diamidino-2-phenylin-dole), and rapid motility of the binucleate organisms was evident. The resulting continuing motility of the organism pre-cluded acquisition of sharp images of the autofluorescence of poorly stained organisms, even after partial arrest of motility using 2,2,2-trichloro-1,1-diol (chloral hydrate) as anaesthetic. These were not useful lumophores for confocal fluorescence microscopy and we present no images. This was particularly disappointing for complex 6^+ in which the reactivity of vinyl group may have aided in targeting specific organelles.

The longer chain variants 2^+–5^+ all revealed good to excel-lent uptake consistent with the highly lipophilic/amphiphilic structures, which will assist passive diffusion across mem-branes. The variation in structure, and amphiphilic nature, however, revealed major differences in the imaging capability across the series. Complex 2^+ was not toxic at the concen-trations used over the duration of the experiment, revealed good uptake and gave very bright images of S. vortens struc-tures, surface and exo-cellular surfaces, e.g. plasma membranes, with minimal penetration into nuclei {Fig. 6(a) and (b)}. The flagellar-driven motility and forward propulsive swimming was maintained across the entire population. Consequently, in order to obtain sharply focused images, it was necessary to anaesthetise using chloral hydrate immedi-ately before microscopical examination. A heterogeneous sized population of Schiz. pombe (a consequence of long and short rods typical of asynchronously dividing individual cells) showed moderate to good uptake of 2^+ in, in particular, younger (shorter) cells with nonspecific localisation within the cell organelles {Fig. 6(c) and (d)}. No localised intense regions of rhenium-based emission were observed in the cytoplasm, indicating non-specific distribution rather than specific uptake in any particular organelles.

As a positive control, ctc (10, Fig. 1, 5-cyano-2,3-di-(p-tolyl) tetrazolium chloride), a cationic organic dye extensively employed in the study of cells as an indicator of cellular redox activity,[31] was used to stain metabolically active cells grown from the same batch. The non-fluorescent compound 10 is reduced in the cell, either via reductase activity or through direct reaction with NADH or NADPH producing an insoluble, deep coloured fluorescent formazan precipitate. It is thought that the positive charge in the tetrazolium is the primary factor responsible for their cellular uptake driven by the plasma and energy-transducing electrochemical membrane potentials.[32] In the aerobically-grown yeast the latter are the mitochondria, whereas in the anaerobic S. vortens, the corres-ponding organelles are the hydrogenosomes.

For S. vortens the ctc/formazan showed good uptake (Fig. 7(a)) and localisation in several organelles including the hydrogenosomes (redox-active organelles equivalent to the mitochondria of aerobic eukaryotic organisms). For Schiz. pombe it again showed good uptake with selective staining of the nuclei {Fig. 7(b) and (c)} within the yeast cells (both nuclei of older elongated cells).

Complex 3^+ was taken up avidly by both S. vortens and Schiz. pombe. It was, however, toxic at the concentrations employed in this study. For S. vortens, background cytosolic binding indicated multiple binding at non-specific locations and images were not clearly defined. For Schiz. pombe, 3^+

Fig. 7 Fluorescence, Normarski DIC and overlaid images of (a) S. vortens containing ctc and (b) and (c) Schiz. pombe containing ctc (scale bars 5 μm).

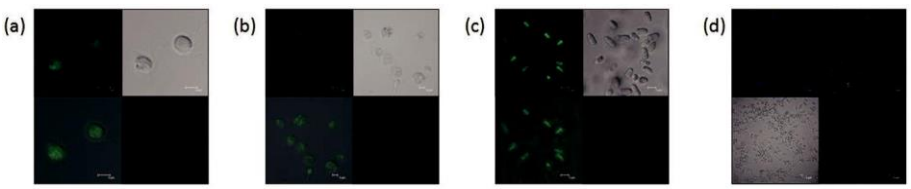

Fig. 6 Fluorescence, Normarski differential interference contrast (DIC) and overlaid images of (a) and (b) S. vortens containing 2^+ and (c) and (d) Schiz. pombe containing 2^+ (scale bars 5 μm).

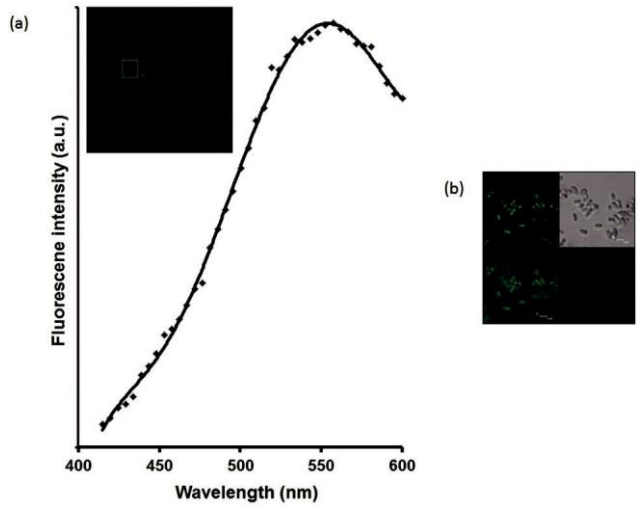

Fig. 8 (a) Fluorescence emission spectrum (λ_{ex} = 405 nm), (inset: range of sample studied) and (b) fluorescence, Normarski DIC, and overlaid images of S. vortens containing 3^+ (scale bars 5 μm).

shows preferential uptake into the nuclei, but also with general background cytosolic labelling. About 30% of popu-lation are faintly phosphorescent (those with very pronounced differential image contrast in walls). A fluorescence emission spectrum from confocal microscopy on a sample region of S. vortens containing 3^+ was recorded (Fig. 8) and revealed a maximum {λ_{max} (em)} around 556 nm, identical to that of the emission wavelength measured by fluorescence spectroscopy for 3^+ in water (Table 5 and ESI†).

For the longer chain variants 4^+ (C_{12}) and 5^+ (C_{16}), the rhenium complexes are toxic at the concentrations used. 4^+ was mounted in 'Vectrashield' containing DAPI. Complex 4^+ showed bright images of S. vortens structures, surface and

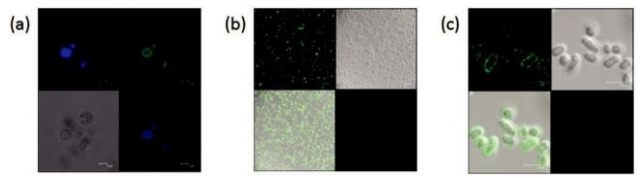

Fig. 9 Fluorescence, Normarski DIC, and overlaid images of (a) S. vortens containing 4^+ and (b) and (c) Schiz. pombe containing 5^+ (scale bars 5 μm).

exocellular surfaces, e.g. plasma membranes, with minimal penetration into nuclei {Fig. 9(a)}. However, staining with complex 5^+ led to complete destruction of all (only one sur-vived intact with unobserved flagella) S. vortens cells (see ESI†). For Schiz. pombe 4^+ shows good uptake with no specific foci of fluorescence (see ESI†) whereas 5^+ is taken up well around the periphery of the cell revealing labelling of the smooth endo-plasmic membranes, including those of the Golgi apparatus with no penetration into the organelles {Fig. 9(b) and (c)}. The rigid exocellular surface of the Schiz. pombe outer wall is most likely responsible for the cells remaining intact.

Finally, we discuss the complexes of moderately lipophilic ligands 1-mesitylimidazole (ImMes) 7^+ and the thiazoles, 4,5-dimethylthiazole (dmt) 8^+ and 4-methyl-5-thiazoleethanol (mte) 9^+. Complexes 7^+–9^+ were not toxic at the concentrations used over the duration of the experiment and it was necessary to anaesthetise using chloral hydrate immediately before microscopical examination. Complex 7^+ revealed good uptake and gave very bright images of S. vortens localising in orga-nelles in middle of the cell {Fig. 10(a)}. However, it was only taken up by very few cells (only those which appear to be in the process of partitioning) of Schiz. pombe giving a hetero-geneous population of stained cells with no specific localis-ation (see ESI†). The complexes bearing thiazole ligands show generally adequate uptake in both S. vortens and Schiz. pombe giving a heterogeneous population for both cells, with 8^+ showing higher concentrations around the cell membrane of S. vortens {Fig. 10(b)} and 9^+ showing slightly greater localis-ation in nucleus {Fig. 10(d)}. Complex 8^+ stained a sub-population of Schiz. pombe, which appears to be only in shorter, recently divided cells (but not all divided cells), with localisation in organelles.

The imaging results presented here suggest that functiona-lised rhenium imidazole/thiazole complexes are useful as bio-compatible fluorophores. The specific nature of the pendant R-group can be used to tune the imaging capability of the com-plexes from poor uptake (1^+ and 6^+) to good uptake/poor local-isation (2^+), to excellent uptake and distinct regions of fluo-rescence (3^+, 4^+ and 8^+). The toxicity of the complexes can be controlled with properties ranging from non-toxic (2^+, 7^+, 8^+ and 9^+), through toxic at the concentrations used (3^+ and 4^+), and toxic with complete destruction of cells (5^+). The increased liphophilic nature of the complexes appears to increase the uptake of the complexes into the cells, but also increases the toxicity of the fluorophores. The imaging results clearly show

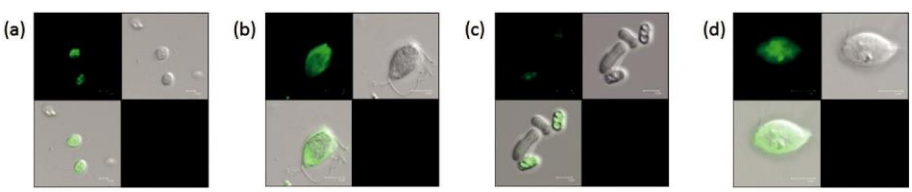

Fig. 10 Fluorescence, Normarski DIC, and overlaid images of (a) S. vortens containing 7^+, (b) S. vortens containing 8^+ (c) Schiz. pombe containing 8^+ and (d) S. vortens containing 9^+ (scale bars 5 μm).

that simple tuning of the amphiphilic nature of the complexes can profoundly alter the uptake, localisation and toxicity of the probes, with the moderately amphiphilic complexes offering the greatest balance between all considerations.

Conclusions

In conclusion, this paper has described the synthesis and structural characterisation of a series of cationic rhenium com-plexes, in which the amphiphilic nature of the complexes is controlled by the variation of the lipophilicity of the axial ligand. The optical properties are dominated by MLCT/LLCT transitions, as predicted by DFT calculations, facilitating visible absorption and effective broad emission characteristics. These properties render the complexes highly compatible with confocal microscopy. Cellular imaging studies were performed on both aerotolerant protistan fish parasite S. vortens and uni-cellular eukaryote "fission yeast" Schiz. pombe showing a large variation in the imaging capabilities. Importantly, the cellular uptake, toxicity and specific localisation can be controlled by the lipophilic nature of the axial ligands. For the complexes described here, the most encouraging results were presented by those complexes of the moderately lipophilic ligands, i.e. good uptake, non-toxic and specific localisation, particularly 7^+ and 8^+ which showed localisation in the nuclei. Complexes of the most lipophilic ligand generally showed localisation within the cell membranes and increasing toxicity with increasing lipophilicity. In addition, under the conditions employed there was little evidence of photobleaching. Therefore by careful selection of the axial ligand this type of complex could be adapted for radioimaging nuclides, for example as ^{99m}Tc(I) compounds, whilst retaining the required physical characteristics for cellular imaging using confocal fluorescence microscopy.

Experimental

All reactions were performed with the use of vacuum line and Schlenk techniques. Reagents were commercial grade and were used without further purification. ^{1}H and ^{13}C–{^{1}H} NMR spectra were recorded on an NMR-FT Bruker 400 MHz or Joel Eclipse 300 MHz spectrometer and recorded in $CDCl_3$. ^{1}H and ^{13}C–{^{1}H} NMR chemical shifts (δ) were determined relative to internal TMS and are given in ppm. Low- and high-resolution mass spectra were obtained by the staff at Cardiff University. UV-Vis studies were performed on a Jasco V-570 spectrophoto-meter as $CHCl_3$ solutions (5×10^{-5} M). Photophysical data were obtained on a JobinYvon-Horiba Fluorolog spectrometer fitted with a JY TBX picoseconds photodetection module as $CHCl_3$ or water/DMSO (98 : 2) solutions. Emission spectra were uncorrected and excitation spectra were instrument corrected. The pulsed source was a Nano-LED configured for 372 nm output operating at 500 kHz. Luminescence lifetime profiles were obtained using the JobinYvon-Horiba FluoroHub single photon counting module and the data fits yielded the lifetime values using the provided DAS6 deconvolution software. Microanalyses were performed by London Metropolitan University, UK.

X-ray data collection and processing

Diffraction data were collected at 100 K on Rigaku AFC12 goniometer equipped with an enhanced sensitivity (HG) Saturn 724+detector mounted at the window of an FR-E+Superbright MoKα (λ = 0.71075 Å) rotating anode genera-tor with HF Varimax optics.[33] X-ray data were recorded and integrated using Rigaku CrystalClear[34] software. Crystal struc-ture was solved by direct methods using SHELXS-2013 [35] and charge flipping methods using SUPERFLIP[36] and refined on F_o^2 by full-matrix least squares refinement using SHELXL-2013/2014 package. All non-hydrogen atoms were refined with anisotropic displacement parameters. All hydro-gen atoms were added at calculated positions and refined using a riding model with isotropic displacement parameters based on the equivalent isotropic displacement parameter (U_{eq}) of the parent atom. Figures were created using the ORTEP3 software package.[37] CCDC depository numbers: 969748, 990428 and 990429.†

DFT studies

Scalar relativistic calculations were performed on the Gaussian 09 program.[38] Geometry optimisations were carried out without constraints using the B3PW91 functional. The LANL2DZ basis set was used for the Re centres, and was invoked with pseudo-potentials for the core electrons, a 6-31G (d,p) basis set for all nitrogen, oxygen and coordinating atoms with a 6-31G basis set for all remaining atoms. All optimis-ations were followed by frequency calculations to ascertain the nature of the stationary point (minimum or saddle point).

Cell culture and imaging

Organisms employed were the fission yeast, Schiz. pombe 972 h-, and the single cell protist fish parasite, S. vortens ATCC 50386. The yeast was grown and maintained on Sabouraud Maltose Agar (Difco) then transferred to unbaffled conical flasks (50 ml) containing 10 ml of YE'PD liquid medium (0.3% yeast extract, 1% peptone and 1% glucose), and grown under aerobic conditions for 2 days on a rotary shaker at 150 rpm. Removal of nutrients was by centrifugation for 3 min at 2000 rpm (3000g) and resuspension in 50 mM phosphate buffer at pH 7.2. S. vortens was grown anaerobically in stop-pered tubes on a rich serum-containing medium, harvested and washed as described previously.[39] Cytotoxicity was deter-mined by exposure to the complexes at 1–100 μM for inhi-bition of growth at intervals for up to 36 h. The homogeneous cell suspension was then distributed into 1 ml aliquots, with each aliquot being subject to incubation with a different imaging probe. These luminescent probes were initially dis-solved in dimethyl sulfoxide (DMSO) (5 mg ml^{-1}) before being added to the cell suspensions, with a final concentration of 100 μg ml^{-1} (corresponding to about 110–190 μM) before incu-

bation at 20 °C for 30 min. While it is known that DMSO can cause instability in biological active metal complexes,[40] in the current work the complexes were found to be stable in DMSO. Cells were finally washed in phosphate buffer saline (PBS, pH 7.2), removing agent from the medium, then harvested by centrifugation (5 min, 800g) and mounted on a slide for imaging. Preparations were viewed using a Leica TCS SP2 AOBS confocal laser scanning microscope with excitation at 405 nm and detection band ranging from 515–600 nm.

Synthesis

ImC_4H_9. Imidazole (5.05 g, 74.18 mmol), bromobutane (8.5 ml, 78.78 mmol) and KOH (5.1 g, 90.91 mmol) were heated in DMF (60 ml) at 120 °C for 16 h. After cooling, water (150 ml) was added and the product was extracted with CH_2Cl_2 (100 ml). The organic phase was separated, washed with water (100 ml) and brine (2 × 100 ml) and dried over $MgSO_4$. After filtering, the solvent was removed in vacuo and the crude product dissolved in toluene before solvent removal in vacuo once more. The product was purified by bulb-to-bulb vacuum distillation using Kügelrohr apparatus to give a colourless oil. Yield = 7.74 g, 62.33 mmol (84%). ^{1}H NMR data were as previously reported.[41]

ImC_8H_{17}, $ImC_{12}H_{25}$ and $ImC_{16}H_{33}$ were prepared similarly from imidazole and 1-bromooctane, 1-bromododecane or 1-bromohexadecane respectively. ^{1}H NMR data were as pre-viously reported.[42]

ImMes. Prepared by slight modification of literature pro-cedure. 2,4,6-trimethylaniline (6.8 g, 0.05 mol) in MeOH (25 mL) was stirred with 30% aqueous glyoxal (8.1 mL, 0.05 mol) for 16 h at room temperature. A bright yellow mixture was formed. Then, NH_4Cl (5.4 g, 0.1 mol) was added followed by 37% aqueous formaldehyde (8 mL, 0.1 mol). The mixture was diluted with MeOH (200 ml) and the resulting mixture was refluxed for 1 h. H_3PO_4 (7 mL, 85% soln.) was added over a period of 10 min. The resulting mixture was then stirred at reflux overnight. After removal of the solvent, the dark residue was poured onto ice (100 g) and bacified with aqueous 40% KOH solution until pH 9. The resulting mixture was extracted with EtOAc (2 × 100 ml). The organic phases were combined and washed with H_2O, brine and dried with anhydrous $MgSO_4$. After filtering, the solvent was removed and the residue was purified by bulb-to-bulb vacuum distillation using Kügelrohr apparatus at 240 °C (some unreacted 2,4,6-tri-methylaniline initially distils as a colourless oil at lower tem-perature). ^{1}H NMR data were as previously reported.[14]

$[Re(CO_3)(bpy)(ImCH_3)]BF_4$ (1^+). $[Re(CO)_3(bpy)(MeCN)]BF_4$ (0.083 g, 0.149 mmol) and 1-methylimidazole (0.014 g, 0.170 mmol) were heated at reflux in $CHCl_3$ for 16 h. The solvent was then removed in vacuo. The product was purified by column chromatography (silica/CH_2Cl_2). Unreacted methyl imidazole was eluted with CH_2Cl_2 and the product as the first yellow band with CH_2Cl_2/MeOH (95 : 5). The product was recrystallised from CH_2Cl_2/Et_2O to give a bright yellow powder. Yield = 0.055 g, 0.091 mmol (61%). ^{1}H NMR (250 MHz, $CDCl_3$) δ_H = 8.91 (2H, d, $^3J_{HH}$ = 4.4 Hz), 8.53 (2H, d, $^3J_{HH}$ = 8.1 Hz), 8.20 (2H, app t. {coincident dd}, $^3J_{HH}$ = 7.8 Hz), 7.56 (2H, app t., $^3J_{HH}$ = 6.3 Hz), 6.88 (1H, broad s), 6.85 (1H, broad s), 6.69 (1H, broad s), 3.49 (3H, s) ppm. ^{13}C NMR (75 MHz, $CDCl_3$) δ_C = 156.3, 152.7, 141.1, 130.9, 129.6, 128.4, 125.8, 122.5, 33.6 ppm. UV-vis ($CHCl_3$): λ_{max} (ε/L mol^{-1} cm^{-1}) 240 (22 900), 282 (17 525), 355 (4800) nm. Elemental analysis: calcd (%) for $C_{17}H_{14}N_4O_3ReBF_4$: C, 34.30, H, 2.37, N, 9.41; found: C, 34.28, H, 2.49, N, 9.38. ES MS found m/z 509.2, calculated m/z 509.1 for $[M - BF_4]^+$. HR MS found m/z 507.0594, calculated m/z 507.0596 for $[C_{17}H_{14}N_4O_3{}^{185}Re]^+$. IR (KBr) ν(CO) = 2026, 1916 cm^{-1}.

$[Re(CO_3)(bpy)(ImC_4H_9)]BF_4$ (2^+). Prepared similarly from $[Re(CO)_3(bpy)(MeCN)]BF_4$ (0.085 g, 0.152 mmol) and ImC_4H_9 (0.019 g, 0.153 mmol). Yield = 0.069 g, 0.108 mmol (71%). ^{1}H NMR (250 MHz, $CDCl_3$) δ_H = 8.90 (2H, d, $^3J_{HH}$ = 4.3 Hz), 8.58 (2H, d, $^3J_{HH}$ = 7.5 Hz), 8.21 (2H, app t., $^3J_{HH}$ = 7.5 Hz), 7.57 (2H, app t., $^3J_{HH}$ = 6.3 Hz), 6.93 (1H, broad s), 6.78 (1H, broad s), 6.73 (1H, broad s), 3.75 (2H, t, $^3J_{HH}$ = 7.5 Hz), 1.10 (2H, m), 0.75 (2H, m), 0.42 (3H, m) ppm. ^{13}C NMR (75 MHz, $CDCl_3$) δ_C = 155.8, 152.6, 141.2, 138.7, 130.7, 128.3, 125.6, 120.6, 48.1, 32.5, 19.5, 13.5 ppm. UV-vis ($CHCl_3$): λ_{max} (ε/L mol^{-1} cm^{-1}) 240 (22 650), 282 (17 950), 355 (4915) nm. Elemental analysis: calcd (%) for $C_{20}H_{20}N_4O_3ReBF_4$: C, 37.69, H, 3.16, N, 8.79; found: C, 37.74, H, 3.07, N, 8.69. ES MS found m/z 551.1, calculated m/z 551.1 for $[M - BF_4]^+$. HR MS found m/z 549.1042, calculated m/z 549.1065 for $[C_{20}H_{20}N_4O_3{}^{185}Re]^+$. IR (KBr) ν(CO) = 2026, 1915 cm^{-1}.

$[Re(CO_3)(bpy)(ImC_8H_{17})]BF_4$ (3^+). Prepared similarly from $[Re(CO)_3(bpy)(MeCN)]BF_4$ (0.080 g, 0.143 mmol) and ImC_8H_{17} (0.031 g, 0.172 mmol). Yield = 0.069 g, 0.099 mmol (69%). ^{1}H NMR (250 MHz, $CDCl_3$) δ_H = 8.93 (2H, d, $^3J_{HH}$ = 4.5 Hz), 8.60 (2H, d, $^3J_{HH}$ = 8.2 Hz), 8.22 (2H, app t., $^3J_{HH}$ = 6.6 Hz), 7.49 (2H, app t., $^3J_{HH}$ = 4.5 Hz), 6.97 (1H, s), 6.71 (2H, broad s), 3.75 (2H, t, $^3J_{HH}$ = 7.4 Hz), 3.41 (2H, app q (coincident tt), $^3J_{HH}$ = 7.40 Hz), 1.25–1.05 (10H, m), 0.81 (3H, t, $^3J_{HH}$ = 7.0 Hz) ppm. ^{13}C NMR (75 MHz, $CDCl_3$) δ_C = 195.2, 191.1, 154.9, 152.3, 140.5, 138.6, 128.6, 127.9, 124.6, 120.4, 47.5, 30.9, 29.8, 28.3, 28.2, 25.5, 21.9, 13.4 ppm. UV-vis ($CHCl_3$): λ_{max} (ε/L mol^{-1} cm^{-1}) 240 (17 400), 276 (18 050), 354 (2600) nm. Elemental analysis: calcd (%) for $C_{24}H_{28}N_4O_3ReBF_4$: C, 41.56, H, 4.07, N, 8.08; found: C, 41.63, H, 4.07, N, 7.92. ES MS found m/z 607.2, calculated m/z 607.2 for $[M - BF_4]^+$. HR MS found m/z 605.1681, calculated m/z 605.1691 for $[C_{24}H_{28}N_4O_3{}^{185}Re]^+$. IR (KBr) ν(CO) = 2027, 1910 cm^{-1}.

$[Re(CO_3)(bpy)(ImC_{12}H_{25})]BF_4$ (4^+). Prepared similarly from $[Re(CO)_3(bpy)(MeCN)]BF_4$ (0.080 g, 0.143 mmol) and $ImC_{12}H_{25}$ (0.034 g, 0.144 mmol). Yield = 0.068 g, 0.090 mmol (63%). ^{1}H NMR (250 MHz, $CDCl_3$) δ_H = 8.91 (2H, d, $^3J_{HH}$ = 4.3 Hz), 8.62 (2H, d, $^3J_{HH}$ = 8.0 Hz), 8.21 (2H, app t., $^3J_{HH}$ = 7.6 Hz), 7.47 (2H, app t., $^3J_{HH}$ = 6.0 Hz), 6.97 (1H, s), 6.73 (2H, 2 × d, $^3J_{HH}$ = 5.1 Hz), 3.77 (2H, t, $^3J_{HH}$ = 7.2 Hz), 1.59–1.46 (6H, m), 1.28–1.03 (14H, m), 0.80 (3H, t, $^3J_{HH}$ = 6.4 Hz) ppm. ^{13}C NMR (75 MHz, $CDCl_3$) δ_C = 196.1, 191.8, 155.8, 152.8, 141.2, 139.0, 130.0, 128.5, 125.7, 121.0, 48.3, 31.9, 30.5, 29.7, 29.6, 29.5, 29.4, 29.3, 29.0, 26.3, 22.7, 14.2 ppm. UV-vis ($CHCl_3$): λ_{max} (ε/L mol^{-1} cm^{-1}) 240 (23 650), 282 (16 420), 354 (4350) nm.

Elemental analysis: calcd (%) for $C_{28}H_{36}N_4O_3ReBF_4 \cdot 3Et_2O$: C, 49.43, H, 6.84, N, 5.76; found: C, 49.44, H, 6.56, N, 6.13. ES MS found m/z 663.2, calculated m/z 663.2 for $[M - BF_4]^+$. HR MS found m/z 661.2297, calculated m/z 661.2317 for $[C_{28}H_{36}N_4O_3{}^{185}Re]^+$. IR (KBr) ν(CO) = 2028, 1925 cm^{-1}.

$[Re(CO_3)(bpy)(ImC_{16}H_{33})]BF_4$ (5^+). Prepared similarly from $[Re(CO)_3(bpy)(MeCN)]BF_4$ (0.100 g, 0.180 mmol) and $ImC_{16}H_{33}$ (0.058 g, 0.198 mmol). Recrystallisation from CH_2Cl_2/Et_2O did not initially precipitate the product, and a lowering of volume by slow evaporation was required. Yield = 0.112 g, 0.139 mmol (77%). ^1H NMR (400 MHz, $CDCl_3$) δ_H = 8.91 (2H, d, $^3J_{HH}$ = 5.5 Hz), 8.59 (2H, d, $^3J_{HH}$ = 8.2 Hz), 8.21 (2H, app t., $^3J_{HH}$ = 8.7 Hz), 7.57 (2H, app t., $^3J_{HH}$ = 7.1 Hz), 6.95 (1H, s), 6.75 (1H, br s), 6.72 (1H, br s), 3.74 (2H, t, $^3J_{HH}$ = 7.4 Hz), 1.53–1.47 (6H, m), 1.23–1.05 (22H, m), 0.81 (3H, t, $^3J_{HH}$ = 7.0 Hz) ppm. ^{13}C NMR (75 MHz, $CDCl_3$) δ_C = 155.2, 152.5, 141.1, 138.9, 130.5, 128.2, 125.9, 120.7, 48.4, 32.2, 30.6, 30.0, 29.7, 29.6, 25.1, 29.4, 29.2, 29.1, 28.6, 27.0, 26.4, 22.9, 22.8, 14.2 ppm. UV-vis ($CHCl_3$): λ_{max} (ε/L mol^{-1} cm^{-1}) 246 (21 650), 282 (20 000), 355 (4450) nm. Elemental analysis: calcd (%) for $C_{32}H_{44}N_4O_3ReBF_4$: C, 47.70, H, 5.50, N, 6.95; found: C, 47.60, H, 5.38, N, 7.04. ES MS found m/z 719.3, calculated m/z 719.3 for $[M - BF_4]^+$. HR MS found m/z 717.2940, calculated m/z 717.2943 for $[C_{32}H_{44}N_4O_3{}^{185}Re]^+$. IR (KBr) ν(CO) = 2027, 1905 cm^{-1}.

$[Re(CO_3)(bpy)(ImC_2H_3)]BF_4$ (6^+). Prepared similarly from $[Re(CO)_3(bpy)(MeCN)]BF_4$ (0.116 g, 0.209 mmol) and 1-vinyl-imidazole (20 μl, 0.221 mmol). Yield = 0.109 g, 0.175 mmol (86%). ^1H NMR (250 MHz, $CDCl_3$) δ_H = 8.90 (2H, d, $^3J_{HH}$ = 6.5 Hz), 8.56 (2H, d, $^3J_{HH}$ = 8.1 Hz), 8.29 (1H, s), 8.21 (2H, app t., $^3J_{HH}$ = 7.8 Hz), 7.58 (2H, app t., $^3J_{HH}$ = 6.6 Hz), 7.05 (1H, br s), 6.73 (1H, br s), 5.45 (1H, dd, $^3J_{HH}$ = 15.7 Hz, $^2J_{HH}$ = 2.3 Hz), 5.45 (1H, dd, $^3J_{HH}$ = 15.7 Hz, $^2J_{HH}$ = 2.3 Hz), 5.45 (1H, dd, $^3J_{HH}$ = 15.7 and 2.3 Hz) ppm. ^{13}C NMR (75 MHz, $CDCl_3$) δ_C = 156.0, 153.1, 141.0, 139.2, 130.1, 128.8, 128.0, 126.0, 116.4, 105.2 ppm. UV-vis ($CHCl_3$): λ_{max} (ε/L mol^{-1} cm^{-1}) 245 (21 125), 276 (13 475), 351 (2400) nm. Elemental analysis: calcd (%) for $C_{19}H_{17}N_4O_3ReBF_4$: C, 35.60, H, 2.32, N, 9.22; found: C, 35.46, H, 2.19, N, 9.27. ES MS found m/z 521.1, calculated m/z 521.1 for $[M - BF_4]^+$. HR MS found m/z 519.0590, calculated m/z 519.0596 for $[C_{18}H_{14}N_4O_3{}^{185}Re]^+$. IR (KBr) ν(CO) = 2023, 1919 cm^{-1}.

$[Re(CO_3)(bpy)(ImMes)]BF_4$ (7^+). Prepared similarly from $[Re(CO)_3(bpy)(MeCN)]BF_4$ (0.105 g, 0.181 mmol) and mesityl-imidazole (ImMes) (0.039 g, 0.210 mmol). Yield = 0.107 g, 0.153 mmol (81%). ^1H NMR (400 MHz, $CDCl_3$) δ_H = 9.07 (2H, d, $^3J_{HH}$ = 5.5 Hz), 8.94 (2H, d, $^3J_{HH}$ = 8.3 Hz), 8.40 (2H, app t. (coincident dd), $^3J_{HH}$ = 7.4 Hz), 7.70 (2H, app t., $^3J_{HH}$ = 7.9 Hz), 7.20 (1H, s), 6.95 (2H, s), 6.83 (1H, br s), 6.58 (1H, br s), 2.33 (3H, s), 1.74 (6H, s) ppm. ^{13}C NMR (75 MHz, $CDCl_3$) δ_C = 156.0, 152.2, 152.1, 141.8, 140.2, 139.5, 134.4, 129.5, 129.1, 128.9, 126.4, 124.0, 21.5, 17.0 ppm. UV-vis ($CHCl_3$): λ_{max} (ε/L mol^{-1} cm^{-1}) 248 (23 675), 273 (22 425), 356 (4300) nm. Elemental analysis: calcd (%) for $C_{25}H_{22}N_4O_3ReBF_4 \cdot 0.5CH_2Cl_2$: C, 42.75, H, 3.17, N, 7.96; found: C, 42.25, H, 3.60, N, 7.82. ES MS found m/z 613.1, calculated m/z 612.6 for $[M - BF_4]^+$. HR MS found m/z 611.1213, calculated m/z 611.1222 for $[C_{25}H_{22}N_4O_3{}^{185}Re]^+$. IR (KBr) ν(CO) = 2027, 1925 cm^{-1}.

$[Re(CO_3)(bpy)(dmt)]BF_4$ (8^+). Prepared similarly from $[Re(CO)_3(bpy)(MeCN)]BF_4$ (0.080 g, 0.143 mmol) and 4,5-dimethyl-thiazole (0.017 g, 0.150 mmol). Yield = 0.080 g, 0.128 mmol (90%). ^1H NMR (250 MHz, $CDCl_3$) δ_H = 8.87 (2H, d, $^3J_{HH}$ = 5.2 Hz), 8.71 (2H, d, $^3J_{HH}$ = 8.5 Hz), 8.26 (2H, app t. (coincident dd), $^3J_{HH}$ = 7.5 Hz), 7.72 (1H, s), 7.61 (2H, app t., $^3J_{HH}$ = 8.0 Hz), 2.44 (3H, m), 2.28 (3H, s) ppm. ^{13}C NMR (75 MHz, $CDCl_3$) δ_C = 155.8, 154.6, 152.8, 150.2, 141.7, 129.1, 128.4, 126.3, 16.7, 12.3 ppm. UV-vis ($CHCl_3$): λ_{max} (ε/L mol^{-1} cm^{-1}) 251 (30 000), 346 (4225) nm. Elemental analysis: calcd (%) for $C_{18}H_{15}N_3O_3SReBF_4$: C, 34.51, H, 2.41, N, 6.71; found: C, 34.45, H, 2.93, N, 6.63. ES MS found m/z 540.0, calculated m/z 540.0 for $[M - BF_4]^+$. HR MS found m/z 538.0368, calculated m/z 358.0364 for $[C_{18}H_{15}N_3O_3S^{185}Re]^+$. IR (KBr) ν(CO) = 2025, 1901 cm^{-1}.

$[Re(CO_3)(bpy)(mte)]BF_4$ (9^+). Prepared similarly from $[Re(CO)_3(bpy)(MeCN)]BF_4$ (0.094 g, 0.170 mmol) and 4-methyl-5-thiazoleethanol (25 μL, 0.208 mmol). Yield = 0.103 g, 0.157 mmol (93%). ^1H NMR (400 MHz, $CDCl_3$) δ_H = 8.95 (2H, d, $^3J_{HH}$ = 5.3 Hz), 8.65 (2H, d, $^3J_{HH}$ = 8.2 Hz), 8.22 (2H, app. t, $^3J_{HH}$ = 7.9 Hz), 7.88 (1H, s), 7.61 (2H, app. t, $^3J_{HH}$ = 7.9 Hz), 3.64 (2H, t, $^3J_{HH}$ = 5.7 Hz), 2.81 (2H, t, $^3J_{HH}$ = 5.7 Hz), 2.37 (3H, s), 3.65 (1H, br s) ppm. ^{13}C NMR (75 MHz, $CDCl_3$) δ_C = 196.2, 190.3, 155.9, 155.6, 153.0, 150.2, 141.4, 132.3, 128.4, 126.4, 61.2, 30.3, 15.4 ppm. UV-vis ($CHCl_3$): λ_{max} (ε/L mol^{-1} cm^{-1}) 253 (25 975), 353 (4800) nm. Elemental analysis: calcd (%) for $C_{19}H_{17}N_3O_4SReBF_4$: C, 34.76, H, 2.61, N, 6.40; found: C, 34.59, H, 2.61, N, 6.28. ES MS found m/z 570.0, calculated m/z 570.0 for $[M - BF_4]^+$. HR MS found m/z 568.0466, calculated m/z 568.0469 for $[C_{19}H_{17}N_3O_4S^{185}Re]^+$. IR (KBr) ν(CO) = 2025, 1915 cm^{-1}.

Conflicts of interest

There are no conflicts to declare.

Acknowledgements

The BBSRC (BB/J020397/1) and the Life Science Research Network Wales (LSRNW) are thanked sincerely for funding. Dr Robert Jenkins and Mr Robin Hicks are also gratefully acknowledged for running mass spectra. We thank the EPSRC for the use of the National Crystallographic Service at the University of Southampton.

Notes and references

1 (a) K. Trickett, D. Z. Xing, J. Eastoe, R. Enick, A. Mohamed, M. J. Hollamby, S. Cummings, S. E. Rogers and R. K. Heenan, Langmuir, 2010, 26, 4732–4737; (b) C. R. van den Brom, M. Wagner, V. Enkelmann, K. Landfester and C. K. Weiss, Langmuir, 2010, 26, 15794–15801; (c) P. Gong,

Z. Y. Chen, Y. Y. Chen, W. Wang, X. S. Wang and A. G. Hu, Chem. Commun., 2011, 47, 4240–4242; (d) P. Mahato, S. Saha, S. Choudhury and A. Das, Chem. Commun., 2011, 47, 11074–11076; (e) T. Owen and A. Butler, Coord. Chem. Rev., 2011, 255, 678–687; (f) C. N. Verani, R. Shanmugam, F. R. Xavier, M. M. Allard and K. K. Kpogo, Dalton Trans., 2013, 42, 15296–15306; (g) C. Cebrian, M. Natali, D. Villa, M. Panigati, M. Mauro, G. D'Alfonso and L. De Cola, Nanoscale, 2015, 7, 12000–12009; (h) J. A. Lebron, F. J. Ostos, M. L. Moya, M. Lopez-Lopez, C. J. Carrasco and P. Lopez-Cornejo, Colloids Surf., B, 2015, 135, 817–824; (i) M. S. Johnson, L. Wickramasinghe, C. Verani and R. M. Metzger, J. Phys. Chem. C, 2016, 120, 10578–10583; (j) Q. Zhu, F. Pan, Y. Tian, W. J. Tang, Y. Yuan and A. G. Hu, RSC Adv., 2016, 6, 29441–29447; (k) H. N. Kagalwala, D. N. Chirdon, I. N. Mills, N. Budwal and S. Bernhard, Inorg. Chem., 2017, 56, 10162–10171; (l) M. Marin-Garcia, N. Benseny-Cases, M. Camacho, J. Suades and R. Barnadas-Rodriguez, Chem. Commun., 2017, 53, 8455–8458; (m) P. Garg, G. Kaur and G. R. Chaudhary, New J. Chem., 2018, 42, 1141–1150.

2 P. C. Griffiths, I. A. Fallis, T. Chuenpratoom and R. Watanesk, Adv. Colloid Interface Sci., 2006, 122, 107–117.

3 (a) G. A. Reitz, J. N. Demas, B. A. Degraff and E. M. Stephens, J. Am. Chem. Soc., 1988, 110, 5051–5059; (b) S. James, K. P. Maresca, J. W. Babich, J. F. Valliant, L. Doering and J. Zubieta, Bioconjugate Chem., 2006, 17, 590–596; (c) A. Coleman, C. Brennan, J. G. Vos and M. T. Pryce, Coord. Chem. Rev., 2008, 252, 2585; (d) S. V. Kumar, W. K. C. Lo, H. J. L. Brooks, L. R. Hanton and J. D. Crowley, Aust. J. Chem., 2016, 69, 489–498; (e) A. Carreno, M. Gacitua, J. A. Fuentes, D. Paez-Hernandez, J. P. Penaloza, C. Otero, M. Preite, E. Molins, W. B. Swords, G. J. Meyer, J. Manuel Manriquez, R. Polanco, I. Chavez and R. Arratia-Perez, New J. Chem., 2016, 40, 7687–7700; (f) F. L. Thorp-Greenwood, Organometallics, 2012, 31, 5686–5692; (g) M. P. Coogan and V. Fernández-Moreira, Chem. Commun., 2014, 50, 384–399; (h) S. Hostachy, C. Policar and N. Delsuc, Coord. Chem. Rev., 2017, 351, 172–188; (i) J. L. Wedding, H. H. Harris, C. A. Bader, S. E. Plush, R. Mak, M. Massi, D. A. Brooks, B. Lai, S. Vogt, M. V. Werrett, P. V. Simpson, B. W. Skelton and S. Stagni, Metallomics, 2017, 9, 382–390.

4 (a) G. A. Reitz, W. J. Dressick, J. N. Demas and B. A. DeGraff, J. Am. Chem. Soc., 1986, 108, 5344–5345; (b) M. M. Saw, P. Kurz, N. Agorastos, T. S. Andy Hor, F. X. Sundram, Y. K. Yan and R. Alberto, Inorg. Chim. Acta, 2006, 359, 4087–4094; (c) E. Boros, U. O. Häfeli, B. O. Patrick, M. J. Adam and C. Orvig, Bioconjugate Chem., 2009, 20, 1002–1009; (d) V. Fernández-Moreira, F. L. Thorp-Greenwood, A. J. Amoroso, J. Cable, J. B. Court, V. Gray, A. J. Hayes, R. L. Jenkins, B. M. Kariuki, D. Lloyd, C. O. Millet, C. Williams and M. P. Coogan, Org. Biomol. Chem., 2010, 8, 3888–3901; (e) S. Clede, F. Lambert, R. Saint-Fort, M. A. Plamont, H. Bertrand, A. Vessieres and C. Policar, Chem. – Eur. J., 2014, 20, 8714–8722; (f) H. C. Bertrand, S. Clede, R. Guillot, F. Lambert and C. Policar, Inorg. Chem., 2014, 53, 6204–6223; (g) G. Balakrishnan, T. Rajendran, K. S. Murugan, M. S. Kumar, V. K. Sivasubramanian, M. Ganesan, A. Mahesh, T. Thirunalasundari and S. Rajagopal, Inorg. Chim. Acta, 2015, 434, 51–59; (h) C. Cebrian, M. Natali, D. Villa, M. Panigati, M. Mauro, G. D'Alfonso and L. De Cola, Nanoscale, 2015, 7, 12000–12009; (i) M. Marín-Garcıa, N. Benseny-Cases, M. Camacho, J. Suades and R. Barnadas-Rodrıguez, Chem. Commun., 2017, 53, 8455–8458.

5 (a) R. G. Balasingham, F. L. Thorp-Greenwood, C. F. Williams, M. P. Coogan and S. J. A. Pope, Inorg. Chem., 2012, 51, 1419–1426; (b) K. Y. Zhang, K. K.-S. Tso, M.-W. Louie, H.-W. Liu and K. K.-W. Lo, Organometallics, 2013, 32, 5098–5102; (c) A. W.-T. Choi, M.-W. Louie, S. P.-Y. Li, H.-W. Liu, B. T.-N. Chan, T. C.-Y. Lam, A. C.-C. Lin, S.-H. Cheng and K. K.-W. Lo, Inorg. Chem., 2012, 51, 13289–13302; (d) M.-W. Louie, A. W.-T. Choi, H.-W. Liu, B. T.-N. Chan and K. K.-W. Lo, Organometallics, 2012, 31, 5844–5855; (e) E. E. Langdon-Jones, N. O. Symonds, S. E. Yates, A. J. Hayes, D. Lloyd, R. Williams, S. J. Coles, P. N. Horton and S. J. A. Pope, Inorg. Chem., 2014, 53, 3788–3797.

6 G. Gasser, S. Neumann, I. Ott, M. Seitz, R. Heumann and N. Metzler-Nolte, Eur. J. Inorg. Chem., 2011, 5471–5478.

7 S. Clède, N. Cowan, F. Lambert, H. C. Bertrand, R. Rubbiani, M. Patra, J. Hess, C. Sandt, N. Trcera, G. Gasser, J. Keiser and C. Policar, ChemBioChem, 2016, 17, 1004–1007.

8 (a) A. Leonidova and G. Gasser, ACS Chem. Biol., 2014, 9, 2180–2193.

9 (a) S. R. Bayly, C. L. Fisher, T. Storr, M. J. Adam and C. Orvig, Bioconjugate Chem., 2004, 15, 923–926; (b) C. M. Chang, K. L. Lan, W. S. Huang, Y. J. Lee, T. W. Lee, C. H. Chang and C. M. Chuang, Int. J. Mol. Sci., 2017, 18, 15; (c) M. Erfani, N. Rahmani, A. Doroudi and M. Shafiei, Nucl. Med. Biol., 2017, 49, 1–7.

10 (a) J. Bowers, C. P. Butts, P. J. Martin, M. C. Vergara-Gutierrez and R. K. Heenan, Langmuir, 2004, 20, 2191–2198; (b) Y. He, Z. Li, P. Simone and T. P. Lodge, J. Am. Chem. Soc., 2006, 128, 2745–2750; (c) N. A. Smirnova, A. A. Vanin, E. A. Safonova, I. B. Pukinsky, Y. A. Anufrikov and A. L. Makarov, J. Colloid Interface Sci., 2009, 336, 793–802; (d) J. Eastoe, S. Gold, S. E. Rogers, A. Paul, T. Welton, R. K. Heenan and I. Grillo, J. Am. Chem. Soc., 2005, 127, 7302–7303; (e) Y. Gao, S. Han, B. Han, G. Li, D. Shen, Z. Li, J. Du, W. Hou and G. Zhang, Langmuir, 2005, 21, 5681–5684; (f) H. Gao, J. Li, B. Han, W. Chen, J. Zhang, R. Zhang and D. Yan, Phys. Chem. Chem. Phys., 2004, 6, 2914–2916; (g) Surfactants Science Series, ed. M. Fanun, CRC Press/ Taylor and Francis Inc., Boca Raton, Florida, USA, 2008, vol. 144, p. 203; (h) Y. Q. Gu, L. J. Shi, X. Y. Cheng, F. Lu and L. Q. Zheng, Langmuir, 2013, 29, 6213–6220.

11 (a) F. Zhou, Y. Liang and W. Liu, Chem. Soc. Rev., 2009, 38, 2590–2599; (b) S. Zhu, Y. Wu, Q. Chen, Z. Yu, C. Wang, S. Jin, Y. Ding and G. Wu, Green Chem., 2006, 8, 325–327; (c) Ionic

Liquids: Applications and Perspectives, ed. A. Kokorin, InTech, 2011, p. 659; (d) A. K. L. Yuen, A. F. Masters and T. Maschmeyer, Catal. Today, 2013, 200, 9.

12 (a) J. D. Holbrey and K. R. Seddon, J. Chem. Soc., Dalton Trans., 1999, 2133–2139; (b) R. Hayes, G. G. Warr and R. Atkin, Chem. Rev., 2015, 115, 6357–6426.

13 (a) C. K. Lee, C. S. Vasam, T. W. Huang, H. M. J. Wang, R. Y. Yang, C. S. Lee and I. J. B. Lin, Organometallics, 2006, 25, 3768–3775; (b) W. J. Sommer and M. Weck, Adv. Synth. Catal., 2006, 348, 2101–2113; (c) S. P. Downing and A. A. Danopoulos, Organometallics, 2006, 25, 1337–1340; (d) F. Almalioti, J. MacDougall, S. Hughes, M. M. Hasson, R. L. Jenkins, B. D. Ward, G. J. Tizzard, S. J. Coles, D. W. Williams, S. Bamford, I. A. Fallis and A. Dervisi, Dalton Trans., 2013, 42, 1237012380.

14 (a) S. Ahrens, A. Peritz and T. Strassner, Angew. Chem., Int. Ed., 2009, 48, 7908–7910; (b) D.-Ho Lee, J.-Ho Kim, B.-H. Jun, H. Kang, J. Park and Y.-S. Lee, Org. Lett., 2008, 10, 1609–1612.

15 J. V. Caspar and T. J. Meyer, J. Phys. Chem., 1983, 87, 952–957.

16 M. A. Huertos, J. Perez and L. Riera, J. Am. Chem. Soc., 2008, 130, 5662–5663.

17 A. Leonidova, V. Pierroz, L. A. Adams, N. Barlow, S. Ferrari, B. Graham and G. Gasser, ACS Med. Chem. Lett., 2014, 4, 809–814.

18 M. Patra, T. Joshi, V. Pierroz, K. Ingram, M. Kaiser, S. Ferrari, B. Spingler, J. Keiser and G. Gasser, Chem. – Eur. J., 2013, 19, 14768–14722.

19 Krause's Food, Nutrition, and Diet Therapy, ed. L. K. Mahan and S. Escott-Stump, W.B. Saunders Company, Philadelphia, 10th edn, 2000.

20 T. A. Oriskovich, P. S. White and H. H. Thorp, Inorg. Chem., 1995, 34, 1629–1631.

21 W. B. Connick, A. J. Di Bilio, M. G. Hill, J. R. Winkler and H. B. Gray, Inorg. Chim. Acta, 1995, 240, 169–173.

22 H. D. Flack and G. Bernardinelli, Acta Cryst., Sect. A: Found. Crystallogr., 1999, 55, 908–915.

23 M. Korth, M. Pitonák, J. Rezác and P. Hobza, J. Chem. Theory Comput., 2010, 6, 344–352.

24 J. J. P. Stewart, MOPAC2012, Stewart Computational Chemistry, Colorado Springs, CO, USA, 2012, http:// OpenMOPAC.net.

25 R. A. Saunders and J. A. Platts, New J. Chem., 2004, 28, 166–172.

26 L. R. Dodd and D. N. Theodorou, Mol. Phys., 1991, 72, 1313–1345.

27 (a) W.-K. Chung, K. M.-C. Wong, W. H. Lam, X. Zhu, N. Zhu, H.-S. Kwok and V. W.-W. Yam, New J. Chem., 2013, 37, 1753–1767; (b) S. Bullock, A. J. Hallett, L. P. Harding, J. J. Higginson, S. A. F. Piela, S. J. A. Pope and C. R. Rice, Dalton Trans., 2012, 41, 14690; (c) F. L. Thorp-Greenwood, M. P. Coogan, A. J. Hallett, R. H. Laye and S. J. A. Pope, J. Organomet. Chem., 2009, 694, 1400–1406; (d) A. J. Hallett, P. Christian, J. E. Jones and S. J. A. Pope, Chem. Commun., 2009, 4278–4280.

28 J. Joule and K. Mills, Heterocyclic Chemistry, Wiley, Chichester, 5th edn, 2010, p. 464.

29 J. R. Lakowicz, Principles of Fluorescence Spectroscopy, Springer, New York, 3rd edn, 2006.

30 M. P. Coogan, V. Fernández-Moreira, J. B. Hess, S. J. A. Pope and C. Williams, New J. Chem., 2009, 33, 1094–1099.

31 (a) J. Prochazkova, D. Marecek and K. Zaydlar, J. Hyg., Epidemiol., Microbiol., Immunol., 1985, 29, 447; (b) J. Stellmach, Histochemistry, 1984, 80, 137–143; (c) J. Stellmach and E. Severin, Histochemistry, 1987, 19, 21–26.

32 M. V. Berridge, P. M. Herst and A. S. Tan, Biotechnol. Annu. Rev., 2005, 11, 127–152.

33 S. J. Coles and P. A. Gale, Chem. Sci., 2012, 683–689.

34 CrystalClear-SM Expert 3.1 b27, Rigaku, 2012.

35 G. M. Sheldrick, Acta Crystallogr., Sect. A: Found. Crystallogr., 2008, 64, 112–122.

36 L. Palatinus and G. Chapuis, Superflip - a computer program for the solution of crystal structures by charge flip-ping in arbitrary dimensions, J. Appl. Crystallogr., 2007, 40, 786–790.

37 L. J. Farrugia, J. Appl. Crystallogr., 1997, 30, 565–565.

38 M. J. Frisch, G. W. Trucks, H. B. Schlegel, G. E. Scuseria, M. A. Robb, J. R. Cheeseman, G. Scalmani, V. Barone, B. Mennucci, G. A. Petersson, H. Nakatsuji, M. Caricato, X. Li, H. P. Hratchian, A. F. Izmaylov, J. Bloino, G. Zheng, J. L. Sonnenberg, M. Hada, M. Ehara, K. Toyota, R. Fukuda, J. Hasegawa, M. Ishida, T. Nakajima, Y. Honda, O. Kitao, H. Nakai, T. Vreven, J. A. Montgomery Jr., J. E. Peralta, F. Ogliaro, M. Bearpark, J. J. Heyd, E. Brothers, K. N. Kudin, V. N. Staroverov, T. Keith, R. Kobayashi, J. Normand, K. Raghavachari, A. Rendell, J. C. Burant, S. S. Iyengar, J. Tomasi, M. Cossi, N. Rega, J. M. Millam, M. Klene, J. E. Knox, J. B. Cross, V. Bakken, C. Adamo, J. Jaramillo, R. Gomperts, R. E. Stratmann, O. Yazyev, A. J. Austin, R. Cammi, C. Pomelli, J. W. Ochterski, R. L. Martin, K. Morokuma, V. G. Zakrzewski, G. A. Voth, P. Salvador, J. J. Dannenberg, S. Dapprich, A. D. Daniels, O. Farkas, J. B. Foresman, J. V. Ortiz, J. Cioslowski and D. J. Fox, Gaussian 09, Revision C.01, Gaussian, Inc., Wallingford CT, 2010.

39 C. O. M. Millet, J. Cable and D. Lloyd, J. Eukaryotic Microbiol., 2010, 57, 400–404.

40 M. D. Hall, K. A. Telma, K.-E. Chang, T. D. Lee, J. P. Madigan, J. R. Lloyd, I. S. Goldlust, J. D. Hoeschele and M. M. Gottesman, Cancer Res., 2014, 74, 3913–3922.

41 L. C. Fidale, S. Possidonio and O. A. El Seoud, Macromol. Biosci., 2009, 9, 813–821.

42 (a) Q.-X. Liu, F.-B. Xu, Q.-S. Li, H.-B. Song and Z.-Z. Zhang, Organometallics, 2004, 23, 610–614; (b) Q.-X. Liu, F.-B. Xu, Q.-S. Li, H.-B. Song and Z.-Z. Zhang, J. Mol. Struct., 2004, 697, 131–135; (c) K. Asano and S. Matsubara, Synthesis, 2009, 3219–3226; M. Lee, Z. Niu, C. Slebodnick and H. W. Gibson, J. Phys. Chem. B, 2010, 114, 7312–7319; (d) M. Tosoni, S. Laschat and A. Baro, Helv. Chim. Acta, 2004, 87, 2742–2749.